JACC: CARDIOVASCULAR IMAGING VOL. 6, NO. 1, 2013

ISSN 1936-878X/$36.00

PUBLISHED BY ELSEVIER INC.

http://dx.doi.org/10.1016/j.jcmg.2012.05.016

Real-Time Integration of MDCT-Derived Coronary Anatomy and Epicardial Fat

Impact on Epicardial Electroanatomic Mapping and Ablation for Ventricular Arrhythmias

Carine F. van Huls van Taxis, MD,* Adrianus P. Wijnmaalen, MD, PhD,* Sebastiaan R. Piers, MD,* Rob J. van der Geest, PhD,† Martin J. Schalij, MD, PhD,* Katja Zeppenfeld, MD, PhD*

Leiden, the Netherlands

OBJECTIVES This study aimed to evaluate the feasibility and accuracy of real-time integration of multidetector computed tomography (MDCT) derived coronary anatomy and epicardial fat distribution and its impact on electroanatomical mapping and ablation.

BACKGROUND Epicardial catheter ablation for ventricular arrhythmias (VA) is an important therapeutic option in patients after endocardial ablation failure. However, epicardial mapping and ablation are limited by the presence of coronary arteries and epicardial fat.

METHODS Twenty-eight patients (21 male, age 59 ± 16 years) underwent combined endo-epicardial electroanatomical mapping. Prior to the procedure, MDCT derived coronary anatomy and epicardial fat meshes were loaded into the mapping system (CARTO XP, Biosense Webster Inc, Diamond Bar, California). Real-time registration of MDCT data was performed after endocardial mapping. The distance between epicardial ablation sites and coronary arteries was assessed by registered MDCT and angiography. After the procedure, mapping and ablation points were superimposed on the MDCT using a reversed registration matrix for head-to-head comparison of mapping data and corresponding fat thickness.

RESULTS Image registration was successful and accurate in all patients (position error 2.8 ± 1.3 mm). At sites without evidence for scar, epicardial bipolar voltage decreased significantly ($p < 0.001$) with increasing fat thickness. Forty-six VA were targeted; 25 (54%) were abolished by catheter ablation, in 21 (46%) ablation failed. In 5 VA no target site was identified and in 3 VA adhesions prevented mapping. In 2 VA ablation was withheld due to His-bundle vicinity and in 7 VA due to proximity of coronary arteries. In 4 VA catheter ablation was ineffective. At ineffective ablation sites epicardial fat was significantly thicker compared to successful sites (16.9 ± 6.8 mm [range 7.3 to 22.2 mm] and 1.5 ± 2.1 mm [range 0.0 to 6.1 mm], $p = 0.002$).

CONCLUSIONS Real-time image integration of pre-acquired MDCT information is feasible and accurate. Epicardial fat >7 mm and the presence of coronary arteries are important reasons for epicardial ablation failure. Visualization of fat thickness during the procedure may facilitate interpretation of bipolar electrograms and identification of ineffective ablation sites. (J Am Coll Cardiol Img 2013;6: 42–52) © 2013 by the American College of Cardiology Foundation

From the *Department of Cardiology, Leiden University Medical Center, Leiden, the Netherlands; and the †Division of Image Processing, Leiden University Medical Center, Leiden, the Netherlands. Dr. van Huls van Taxis is supported by the Netherlands Heart Society (grant 2008B074). Dr. van der Geest is a consultant for Medis Medical Imaging Systems. Dr. Schalij received unrestricted departmental grants from Medtronic, Boston Scientific, and Biotronik. All other authors have reported that they have no relationships relevant to the contents of this paper to disclose.

Manuscript received March 7, 2012; revised manuscript received May 7, 2012; accepted May 17, 2012.

Epicardial electroanatomic mapping (EAM) followed by radiofrequency catheter ablation is an important therapeutic option in patients after endocardial ablation failure. However, despite the presence of a subepicardial substrate, epicardial EAM and ablation may have important limitations. Bipolar voltage mapping might not be accurate to delineate subepicardial scar and can overestimate its extent, as even thin layers of epicardial fat attenuate bipolar voltage (1–3).

See page 53

Once a potential ablation target site (TS) has been identified, ablation needs to be withheld in the vicinity of coronary arteries, usually visualized by repeated coronary injections, or it may not be effective due to thick epicardial fat, the presence of which can only be assumed when irrigated-tip ablation is ineffective (3,4). Cardiac multidetector computed tomography (MDCT) can reliably visualize coronary arteries and epicardial fat (5,6). Accurate real-time integration of MDCT-derived coronary anatomy and fat distribution during the ablation procedure is therefore desirable.

The purpose of this study was: 1) to evaluate epicardial fat distribution in patients undergoing combined endo-epicardial mapping and ablation; 2) to assess the feasibility and accuracy of real-time integration of MDCT-derived coronary anatomy and fat distribution with EAM; 3) to determine the influence of fat thickness on epicardial bipolar and unipolar voltage and ablation outcome; and 4) to evaluate the potential use of integrated MDCT to identify inappropriate ablation sites.

METHODS

Patients and baseline evaluation. The study population consisted of 28 consecutive patients (21 male, 59 ± 16 years of age) scheduled for combined endo-epicardial EAM and ablation (7–9). Ethics committee approval was not necessary because all performed procedures were part of routine clinical protocol. Informed consent was obtained from all patients. Before the procedure, patients underwent transthoracic echocardiography. When considered necessary, magnetic resonance imaging and/or nuclear imaging were performed to determine the presence of structural heart disease.

Pre-procedural MDCT acquisition and processing. Patients underwent cardiac MDCT before EAM using either a 64-detector row helical scanner (Aquillion 64; Toshiba multi-detector, Toshiba Medical Systems, Otawara, Japan) or a 320-detector row volumetric scanner (Aquillion ONE, Toshiba Medical Systems). The patients' heart rate and blood pressure were monitored before the scan. In case of a heart rate ≥65 beats/min and in the absence of contraindications, a beta-blocker was administered (metoprolol 50 to 100 mg orally or 5 to 10 mg intravenously). Scan parameters depended on body posture. For the 64-row contrast-enhanced scan, collimation was 64 × 0.5 mm, the tube voltage was 100 to 135 kV, and the tube current was 250 to 350 mA. For the 32-row contrast-enhanced scan, the heart was imaged in a single heartbeat using prospective triggering with the exposure interval depending on the heart rate. Scan parameters were as follows: 350-ms gantry rotation time, 100 to 135-kV tube voltage, and a tube current of 400 to 580 mA. For both scans, contrast material (Lomeron 400, Bracco, Milan, Italy) was administered, 80 to 110 or 60 to 90 ml, respectively, followed by saline solution flush (5).

The MDCT data were analyzed using MASS software (V2009-EXP LKEB, Leiden, the Netherlands). The aortic, endocardial, pericardial, and epicardial contours and the left main artery (LM) were traced (Fig. 1A). The distance between the epicardial and pericardial contours was computed to assess epicardial fat thickness. A bull's eye reconstruction of the epicardial surface was created and divided into 3 equal long-axis segments (basal, mid, and apical) and 8 equal short-axis segments A through H (6). For each segment, the mean epicardial fat thickness was calculated. The contours were converted into 3-dimensional meshes that could be imported into the EAM system (CARTO XP, Biosense Webster Inc, Diamond Bar, California). The vertices of the epicardial surface mesh were color-coded for fat thickness (Fig. 1B). In addition, the original cardiac MDCT data were loaded into the CARTO system, and cardiac structures were segmented. Before mapping, all meshes and the segmented images were merged to a final fusion image (FFI) using CARTO-Merge (IPE) software, enabling the registration and fusion of multiple datasets (Fig. 1C). After the procedure, all mapping and ablation points and registration matrix were exported from the CARTO system and superimposed on the corresponding short-axis MDCT slice using reversed registration (Fig. 1D).

ABBREVIATIONS AND ACRONYMS

EAM = electroanatomic mapping
FFI = final fusion image
LM = left main artery
LV = left ventricle
MDCT = multidetector computed tomography
RV = right ventricle
TS = target site
VA = ventricular arrhythmia

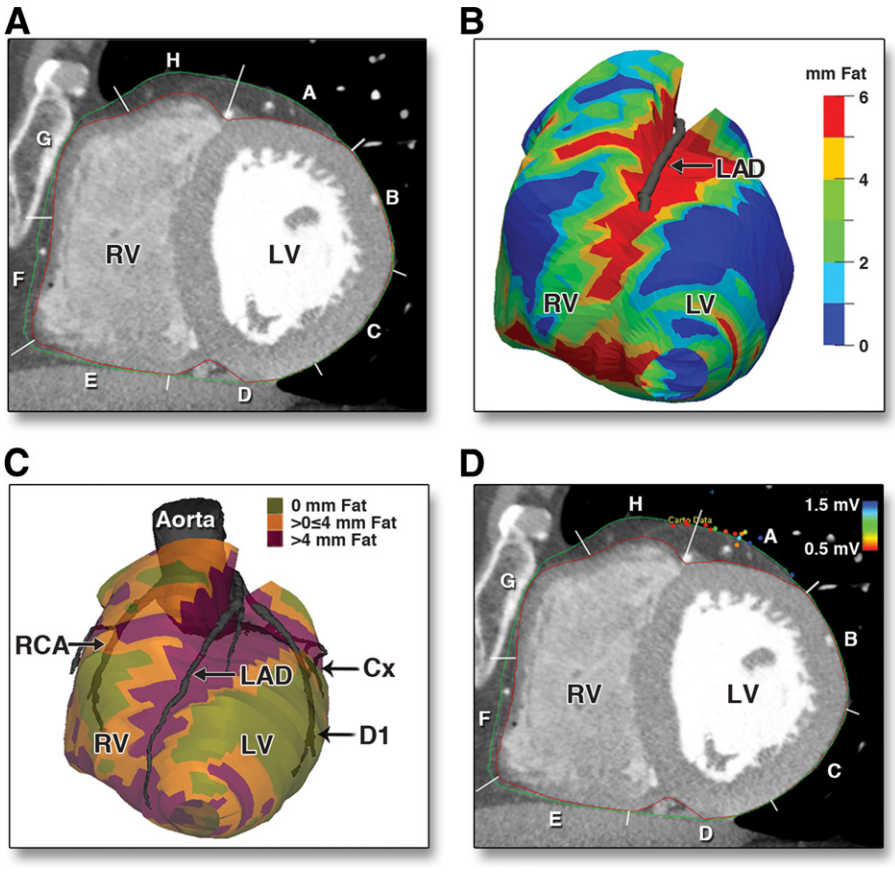

Figure 1. Processing and Integration of MDCT

(A) Multidetector computed tomography (MDCT) short-axis slice with pericardial **(green)** and epicardial **(red)** contours divided into 8 segments **(A through H)**. **(B)** Three-dimensional epicardial surface mesh color-coded for fat thickness. **(C)** MDCT-derived aorta with coronary arteries merged with the epicardial fat meshes (color-coded for fat thickness as indicated) into the final fusion image. **(D)** Same short-axis slice as in **A** with reversed registration of epicardial mapping points projected on the corresponding MDCT location. Points are color-coded for bipolar voltage (color bar). Cx = circumflex coronary artery; D1 = first diagonal coronary artery; LAD = left anterior descending artery; LV = left ventricle; RCA = right coronary artery; RV = right ventricle.

Electrophysiological evaluation. Patients underwent programmed electrical stimulation and combined endo-epicardial EAM. Antiarrhythmic drugs were discontinued for 5 half-lives, except for amiodarone (n = 7). Stimulation consisted of 3 drive-cycle lengths, ≥3 ventricular extra stimuli, and burst pacing at 2 right ventricular sites.

Electroanatomic mapping and real-time image integration. Pericardial access was obtained through a subxiphoid puncture (n = 26) or by a surgical subxiphoidal window because of pericardial adhesions (n = 2) (10). Limited EAM of the aortic root was performed with a 3.5-mm, irrigated-tip catheter (NaviStar ThermoCool, Biosense Webster Inc). The mapping catheter was positioned in the ostium of the LM, confirmed by contrast injection through the catheter, and the location was tagged on the map (11). Second, an endocardial EAM of the left ventricle (LV) and/or right ventricle (RV) was created. Electrograms were filtered at 30 to 400 Hz (bipolar) and 1 to 240 Hz (unipolar). Bipolar voltages <1.5 mV were considered abnormal and <0.5 mV dense scar (12). The MDCT-derived images were aligned with the EAM using the LM location as a landmark for registration (11). Subsequently, the surfaces of the left or right ventricle were aligned using CARTO-Merge software. Distances between the EAM and the FFI were calculated to evaluate registration accuracy.

Identification of target sites. In idiopathic ventricular arrhythmia (VA), LV, RV, aortic sinus, and/or coronary venous system activation mapping was performed. If no TS could be identified, the potential epicardial TS was predicted based on the spatial distribution of earliest local activation time (13).

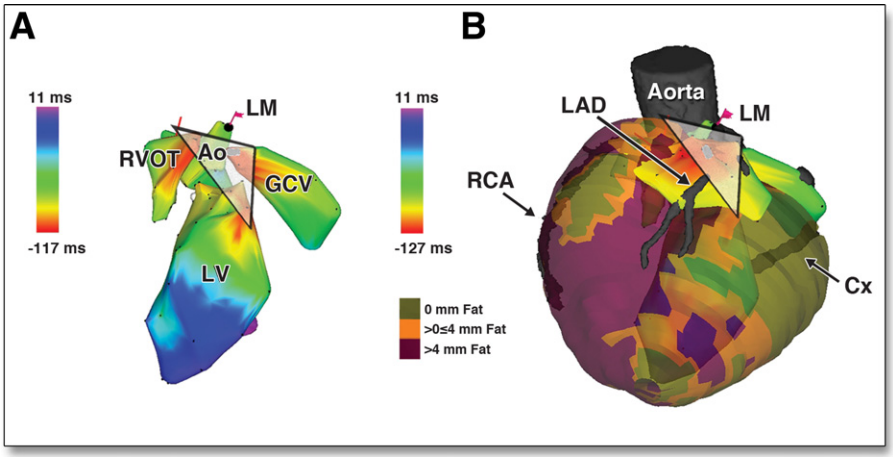

Figure 2. Image Integration: EAM and Predicted Target Site in Relation to MDCT-Derived Epicardial Fat Thickness and Coronary Artery Anatomy

(A) Endocardial electroanatomical activation maps of the LV, right ventricle outflow tract (RVOT), aorta (Ao), and great cardiac vein (GCV). Similar activation time of the LV, RVOT, and GCV was observed. The **white triangle** demonstrates the predicted epicardial target site in the vicinity of the LAD, covered by >4 mm of fat. **(B)** The final fusion image was registered with the endocardial maps, using the left main coronary artery (LM) landmark. Limited epicardial activation mapping confirmed the earliest activation within the predicted site not suitable for ablation. Abbreviations as in Figure 1.

The local fat thickness and proximity of coronary arteries was assessed before epicardial mapping (Fig. 2A).

For scar-related VA, TSs were selected based on activation and entrainment mapping for tolerated VA. For nontolerated VA, TSs were identified guided by pace mapping (≥11/12 lead match between VA-QRS interval, stimulus-to-QRS interval >40 ms) and the presence of late potentials (potentials separated by an isoelectric segment >20 ms and inscribing after the QRS interval.

Epicardial mapping and ablation. For idiopathic VA, limited epicardial voltage mapping was performed, followed by activation mapping. In scar-related VA, a regional epicardial voltage map of the target area was created.

Before epicardial ablation, the vicinity of coronary arteries was estimated on the FFI and categorized into 3 categories (<5 mm, 5 to 15 mm, >15 mm). Subsequently, coronary angiography (left anterior oblique 45°, right anterior oblique 30°) was performed, and the distance between the catheter tip and coronary artery was evaluated on fluoroscopy using the length of the distal electrode pair (6.7 mm) and tip to proximal electrode distance (14.9 mm) as a visual reference (Fig. 3). The distances between the catheter tip and major coronary arteries on the FFI and fluoroscopy were compared to further evaluate the registration accuracy. If TSs were in close proximity to a major branch, additional injections were performed to confirm the accuracy of the spatial relationship as measured on the FFI. Ablation was withheld when the estimated distance was <5 mm. High-output pacing was performed to determine the location of the phrenic nerve, if appropriate.

Radiofrequency energy was applied at 30 to 45 W (maximum temperature, 45°C; flow, 20 to 30 ml/min for 60 s) for endocardial TSs and ≤50 W (flow 20 ml/min) for epicardial TSs until pacing failed to capture and/or elimination of late potentials. Successful ablation sites were defined as sites where ablation terminated the VA and prevented reinducibility. When short linear lesions were applied, the ablation site was deemed successful if the VA was not inducible after ablation. In case the VA remained inducible after ablation, the ablation site was considered unsuccessful. The endpoint of the procedure was noninducibility of any VA, inability to identify TSs, or TS locations that prevented effective or did not allow radiofrequency delivery.

Follow-up. After discharge, patients were followed regularly at our outpatient clinic. Implantable cardioverter-defibrillator interrogation was performed every 6 months. Therapy was regarded appropriate when delivered in response to any VA.

Post-procedural evaluation of the impact of epicardial fat. After the procedure, using the reversed registration, bipolar and unipolar voltages were correlated with epicardial fat thickness using only map-

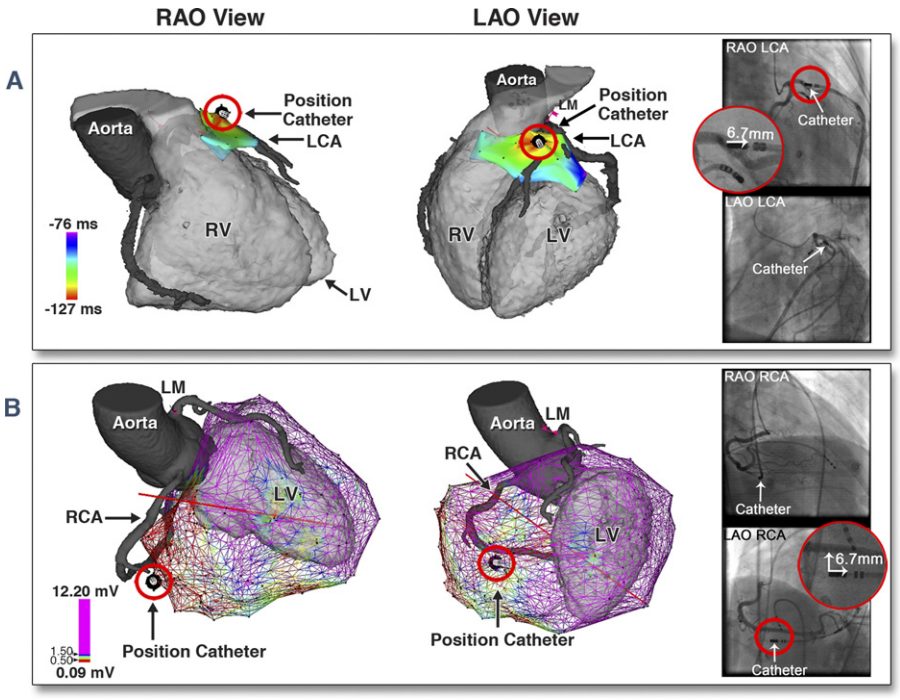

Figure 3. Registration Accuracy: Comparing Image Integration With Coronary Angiography

Registration accuracy in 2 patients comparing the distance between the catheter tip and coronary arteries on integrated MDCT images and coronary angiography in a right anterior oblique (RAO) view **(left)** and left anterior oblique (LAO) view **(right)**. **(A)** Limited activation mapping identified a target site located on the left coronary artery (LCA) on both MDCT and angiography. **(B)** The target site (based on pace mapping) was located <7 mm from the RCA confirmed by angiography. Abbreviations as in Figures 1 and 2.

ping points at sites with no evidence of scar on imaging. Mapping points were grouped into 3 categories according to fat thickness (0 mm, >0 to ≤4 mm, and >4 mm fat) (4). To investigate the impact of epicardial fat on ablation outcome, fat thickness at successful and unsuccessful ablation sites was compared.

Statistical analysis. Statistical analysis was performed using SPSS, version 18.0 (SPSS, Inc., Chicago, Illinois). Continuous variables are expressed as mean ± SD or median (interquartile range [IQR]) when appropriate, and categorical variables as frequency (%). The Mann-Whitney *U* test was used to compare continuous variables between groups. Furthermore, the minimum and maximum value for epicardial fat thickness was noted at successful and unsuccessful TSs. All tests were 2 tailed, and a p value <0.05 was considered statistically significant.

RESULTS

Baseline characteristics and pre-procedural MDCT processing. Baseline patient characteristics are summarized in Table 1. The epicardial surface covered by fat was 65 ± 16%; 25 ± 15% was covered by >4 mm of fat. The basal and apical anterior RV wall and the basal superior LV wall showed the thickest epicardial fat layer (5 to 6 ± 3 mm) (Fig. 1, Online Appendix).

Real-time image integration and registration accuracy. Endocardial voltage maps of the LV were obtained in 25 patients (structural heart disease, 105 ± 65 mapping points; idiopathic, 50 ± 25 mapping points) with an additional RV map in 9. In 3 patients, only RV mapping was performed (67 ± 23 points). Epi-

Table 1. Patient Characteristics

Male	21 (75)
Age, yrs	59 ± 16
LV ejection fraction, %	46 ± 12
Etiology	
Idiopathic	7 (25)
Ischemic	2 (7)
ARVC	3 (11)
LV cardiomyopathy	10 (36)
Biventricular cardiomyopathy	6 (21)

Values are n (%) or mean ± SD.
ARVC = arrhythmogenic right ventricle cardiomyopathy; LV = left ventricle.

cardial mapping was performed in all patients (structural heart disease, 150 ± 74 points; idiopathic, 87 ± 50 points). The MDCT-derived images were successfully integrated with the aortic and LV and/or RV EAM with a surface registration error of 2.8 ± 1.3 mm.

Target sites and procedural outcome. In 22 patients, 41 VAs (cycle length, 382 ± 98 ms) were induced; in 5 patients, the clinical VA (idiopathic premature ventricular contractions) was present at baseline and in 1 patient, no VA could be induced. All VAs were targeted (Table 2). Seven VAs (15%) in 5 patients were successfully ablated from the endocardium, and 18 VAs (39%) in 13 patients were successfully ablated from the epicardium (7.7 ± 4.3 applications/VA). Ablation of 21 VAs (46%) in 13 patients was unsuccessful, mainly due to ineffective ablation or proximity of the TS to coronary arteries.

Use of MDCT-derived coronary anatomy and epicardial fat distribution. To further evaluate registration accuracy, the distances between 28 TSs and coronary arteries on the FFI and coronary angiography were compared. In all cases, the distance was confirmed by angiography (Fig. 3, Table 2). In 2 patients, ablation was successfully performed without acute complications despite the vicinity of coronary arteries; 1 patient had a TS near a functional occluded coronary artery, and the other was in cardiogenic shock because of incessant ventricular tachycardia. This patient died 6 weeks later of progressive heart failure. No coronary artery lesion could be detected at autopsy (Fig. 2, Online Appendix). Ineffective ablation sites were covered by >4 mm of fat (as delineated by the fat meshes) and located at the LV superior wall and RV anterior superior wall.

Procedural complications. In 1 patient, epicardial bleeding (>80 cm^3) occurred. There was no LM damage as evaluated by angiography or procedure-related death. Procedural time was 253 ± 89 min, and fluoroscopy time was 43 ± 15 min.

Follow-up. During a mean follow-up of 27 ± 15 months, 5 patients died (4 of heart failure and 1 of cancer), and 1 patient underwent heart transplantation because of terminal heart failure. Of the remaining 22 patients, 11 patients experienced VA recurrence, all 7 patients with failed ablation (100%) and 4 (27%) who were noninducible for any VA.

Post-procedural evaluation of the impact of epicardial fat. A total of 1,046 epicardial mapping points were acquired at sites without evidence of scar. Twenty-two percent of these mapping points (n = 232) were located at epicardium not covered by fat with a median bipolar voltage of 2.5 mV (IQR: 1.4 to 4.6 mV) and a median unipolar voltage of 7.5 mV (IQR; 5.4 to 12.0 mV). Bipolar voltages decreased significantly with increasing fat thickness according to the predefined categories ($p < 0.001$) (Fig. 4A). However, 33% of mapping points at areas covered by >4 mm of fat showed bipolar voltages >1.5 mV (Fig. 4B); using the previously suggested cutoff value of 2.8 mm, only 37% of mapping points had bipolar voltage >1.5 mV (3). Unipolar voltage was not influenced by fat (Fig. 4C). Epicardial fat thickness was 19.0 mm (IQR: 9.7 to 21.9 mm; minimum, 7.3 mm and maximum, 22.2 mm) at 4 unsuccessful ablation sites compared with 0.4 mm (IQR: 0.0 to 2.8 mm; minimum, 0.0 mm and maximum, 6.1 mm) at 17 successful ablation sites ($p = 0.002$).

Predicted epicardial target sites in idiopathic VA. In the 7 idiopathic patients, the earliest local activation was similar over a broad endocardial area (Δ local activation ≤10 ms at ≥3 endocardial points >1.5 cm apart) (n = 2), at 2 remote endocardial sites (Δ local activation ≤10 ms at 2 endocardial points >1.5 cm apart) (n = 1), or at both an endocardial and aortic sinus/cardiac venous site (n = 4), suggesting an epicardial TS. The predicted potential epicardial TS after endocardial/aortic/cardiac venous system mapping and its distance to the coronary arteries and fat thickness was confirmed after epicardial EAM and reversed registration in all patients. The area was located near (<5 mm) a coronary artery in 2 patients (no ablation) (Fig. 2B). In 2 patients, the TS was covered by 21.0 to 22.2 mm of fat, and ablation was ineffective. In 3 patients, the TS was located remote (range, 7.3 to 11.5 mm) from a coronary artery and covered by 3.8 ± 2.3 mm of fat. Ablation at these sites abolished the VA.

DISCUSSION

The distribution of epicardial fat and coronary anatomy varies among patients. Both are of key relevance during epicardial mapping and ablation. This study is the first to demonstrate the feasibility and accuracy of real-time integration of MDCT-derived images to visualize both the coronary anatomy and fat distribution even before epicardial mapping. In 62% of patients with failed epicardial ablation, lack of success was related to the proximity of a coronary artery or thick fat layer correctly identified using image integration.

Accuracy of real-time image integration. Image integration was performed using the LM as a single landmark and the surface registration tool provided by

Table 2. Procedural Characteristics

Pt. #	Age, yrs/Sex	BMI, kg/m^2	Etiology	Induced VA/Pt	VA CL, ms	Mapping Strategy	Epicardial Mapping Points	Target Site	Fat Thickness at TS, mm	Ablation Outcome	Failure Reason	Vicinity to Coronary Artery, mm
1	68/M	27.5	Idiopathic	1	PVC	A	106	LV superior	22.2 ± 3.6	Failure	Ablation ineffective	LAD 5–15
2	76/M	19.9	LV CMP	1	300	A+S	187	NI	NA	Failure	Unstable VA, no TS	NA
3	72/M	24.9	LV CMP	2	270	A+S	173	LV inferolateral	2.2 ± 2.1	Success		>15
					322	A+S		LV inferior	1.3 ± 0.7	Success		>15
4	57/F	19.8	Idiopathic	1	504	A	128	LV inferolateral	4.8 ± 0.2	Success		RCA 5–15
5	59/M	24.9	ARVC	1	480	A+S	112	RV anterosuperior	3.3 ± 1.1	Success		RCA 5–15
6	62/M	34.7	LV CMP	2	415	A+S	190	Septal	NA	Failure	TS near His	NA
					405	A+S		Septal	NA	Failure	TS near His	NA
7	18/M	20.9	Idiopathic	1	260	A	154	LV inferolateral	1.2 ± 0.6	Success		RCA 5–15
8	22/M	18.8	ARVC	2	240	A+S	259	NI	NA	Failure	Unstable VA, no TS	NA
					190	A+S		NI	NA	Failure	Unstable VA, no TS	NA
9	40/M	19.9	Biventricular CMP	0	—	S	246	NA	NA	—		NA
10	62/M	23.1	Ischemic	1	440	A+S	220	LV superolateral	0.4 ± 0.0	Success		>15
11	73/M	21.2	LV CMP	1	458	A+S	189	LV inferior	5.4 ± 2.6	Failure	TS near RCA	RCA <5
12	74/M	23.3	Ischemic	1	310	A	182	RV diaphragmatic	6.1 ± 3.4	Success		Occluded LAD <5
13	30/F	19.6	LV CMP	2	243	S	172	LV superolateral	0	Success		>15
					353	A+S		LV superolateral	0	Success		>15
14	48/F	22.1	ARVC	2	253	A+S	97	RV superior	0	Success		>15
					250	A+S		RV superior	0	Success		>15
15	61/M	31.8	Biventricular CMP	2	360	A+S	37	RV anteroinferior	7.3 ± 1.1	Failure	Ablation ineffective	RCA 5–15
					360	A+S		RV anteroinferior endocardial	NA	Success		NA
16	48/M	19.7	LV CMP	4	520	A+S	176	LV superolateral endocardial	NA	Success		NA
					380	A+S		LV superolateral endocardial	NA	Success		NA
					430	A+S		LV inferior endocardial	NA	Success		NA
					430	A+S		LV inferolateral	0.4 ± 1.0	Success		>15
17	65/M	29.7	Idiopathic	1	PVC	A	93	LV superior	10.8 ± 5.8	Failure	TS near LAD	LAD <5
18	45/M	26.7	LV CMP	4	340	S	92	LV superolateral	0.3 ± 0.3	Success		>15
					400	S		NI	NA	Failure	Pericardial adhesions	NA
					440	S		NI	NA	Failure	Pericardial adhesions	NA
					300	S		NI	NA	Failure	Pericardial adhesions	NA

Continued on next page

Table 2. ***continued***

Pt. #	Age, yrs/Sex	BMI, kg/m^2	Etiology	Induced VA/Pt	VA CL, ms	Mapping Strategy	Epicardial Mapping Points	Target Site	Fat Thickness at TS, mm	Ablation Outcome	Failure Reason	Vicinity to Coronary Artery, mm
19	77/F	22.5	Biventricular CMP	1	554	A+S	163	LV superolateral	0	Success		Circumflex artery <5; ablation not withheld
20	70/M	23.1	Biventricular CMP	1	230	S	18	RV anterosuperior endocardial	NA	Success		
21	71/M	34.3	LV CMP	4	387	A+S	68	LV superior	1.3 ± 1.2	Failure	TS near LAD	LAD <5
					621	A+S		LV superior	1.3 ± 1.2	Failure	TS near LAD	LAD <5
					356	A+S		LV superior	1.3 ± 1.2	Failure	TS near LAD	LAD <5
					387	A+S		LV superior	1.3 ± 1.2	Failure	TS near LAD	LAD <5
22	54/M	26.8	Idiopathic	1	PVC	A	61	LV superior	21.0 ± 5.0	Failure	Ablation ineffective	RCA 5–15
23	69/M	28.4	Biventricular CMP	1	350	A+S	80	RV anteroinferior endocardial	NA	Success		
24	71/M	38.7	LV CMP	1	375	A+S	50	LV superior	17.1 ± 2.0	Failure	Ablation ineffective	LAD 5–15
25	66/F	24.2	Biventricular CMP	2	500	A+S	273	LV inferior	0.1 ± 0.3	Success		>15
					430	A+S		RV superior	0.7 ± 1.4	Success		>15
26	69/M	24.0	Idiopathic	1	PVC	A	33	LV superior	5.5 ± 0.3	Success		LAD 5–15
27	59/F	25.5	LV CMP	4	430	S	159	LV superolateral endocardial	NA	Success		NA
					360	S		LV inferolateral endocardial	NA	Success		NA
					350	S		NI	NA	Failure	Unstable VA, no TS	NA
					280	S		NI	NA	Failure	Unstable VA, no TS	NA
28	57/F	36.8	Idiopathic	1	PVC	A	32	LV superior	20.2 ± 7.6	Failure	TS near LAD	LAD <5

A = activation mapping; BMI = body mass index; CL = cycle length; CMP =cardiomyopathy; F = female; LAD = left anterior descending artery; M = male; NA = not applicable; NI = not identified; Pt = patient; PVC = premature ventricular contraction; RCA = right coronary artery; RV = right ventricle; S = substrate mapping; TS = target site; VA = ventricular arrhythmia; other abbreviations as in Table 1.

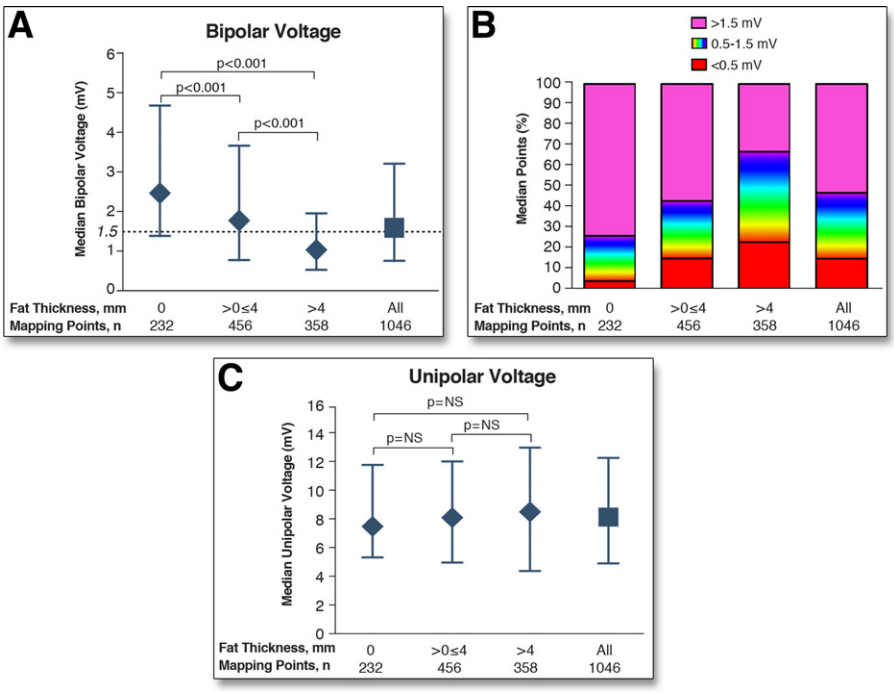

Figure 4. Reversed Registration: Impact of Epicardial Fat on Bipolar and Unipolar Voltages

(A) Median bipolar voltage of epicardial mapping points according to the 3 epicardial fat thickness categories. **(B)** Distribution of epicardial mapping points for each epicardial fat thickness category according to the currently used cutoff values for bipolar voltage mapping. **(C)** Median unipolar voltage of epicardial mapping points according to the 3 epicardial fat thickness categories.

the CARTO system after limited endocardial mapping. This approach resulted in highly accurate integration of MDCT data, verified by surface registration statistics with a mean surface registration error of only 2.8 mm. After confirmation of the registration accuracy by a single coronary injection, the distance between TSs and coronary arteries can be accurately assessed on integrated MDCT. In all 14 patients in whom the TS was located near a coronary artery, the distance was estimated correctly. Therefore, in most cases, the decision to perform ablation can be solely based on the MDCT image integration. However, when MDCT image integration demonstrates the TS to be in close proximity to a relevant coronary artery branch, additional limited coronary injections may still be necessary.

The demonstrated correspondence of the distance between the catheter position and coronary arteries on integrated MDCT and angiography has important practical implications. After confirmation of the registration accuracy by a single coronary injection, the distance between TSs and coronary arteries can be evaluated by integrated MDCT only. Although additional limited contrast injections may still be necessary in case of a TS close to a major branch or when small arteries, such as diagonal and obtuse marginal branches, are not accurately visualized on MDCT, in most cases, image integration is likely to prevent multiple coronary injections at different angulations. It may even enable more accurate assessment of the proximity of a coronary artery if angiography at some angles is limited by the location triangle of the EAM system.

Epicardial fat and voltage mapping. As many as 64% of the epicardial surface was covered with fat and 25% with a fat layer >4 mm. Epicardial fat was not restricted to the atrio- and interventricular groove, as assumed by others (1–3). It can attenuate bipolar voltages, thus preventing accurate delineation of subepicardial scar by bipolar voltage mapping. A fat layer ≥2.8 mm was suggested to best separate low voltage (<1.5 mV) from normal voltage in a previous study (3). However, our newly proposed technique of reversed registration allowed a head-to-head comparison of local voltage data and fat thickness. Although we could confirm a decrease in bipolar voltages with increasing fat thickness, as many as 60% of mapping points acquired in areas with fat and >37% of points acquired in areas with ≥2.8 mm of fat showed normal bipolar voltages.

These findings underscore the importance of accurate MDCT-derived fat information to avoid underestimation of the presence of a significant epicardial fat layer.

In contrast to previous observations, this study demonstrates that unipolar voltage is not influenced by epicardial fat, which may be caused by the larger field of view (3,14,15). Therefore, unipolar voltage mapping may be useful for identification of subepicardial or intramural scar even when thick fat is present.

Epicardial fat and the impact on ablation. Epicardial fat was thickest at the LV superior and RV anterior walls, which is in line with previous investigations (6). Of interest, all ineffective ablation lesions were located in these areas. In a previous study, epicardial cooled-tip ablation was unable to produce lesions when applied at sites covered by a fat layer >3.5 mm (4). However, this was tested for only 3 applications in an animal model. In humans, Desjardins et al. (3) compared the fat thickness of 12 effective and 4 ineffective epicardial cooled-tip ablation sites; all ineffective ablation sites were covered by 10.8 to 14.6 mm fat, whereas effective ablation sites were all located at sites covered by <1.8 mm of fat. Therefore, a cutoff value for epicardial fat thickness precluding effective ablation remained undetermined.

In the current study, ablation was performed at 21 epicardial sites covered by 0 to 22.2 mm of fat, including 6 sites covered by 3.0 to 10.0 mm of fat. Fat thickness at ineffective ablation sites ranged from 7.3 to 22.2 mm. In contrast, all effective ablation sites were covered by 0 to 6.1 mm of fat. These findings suggest that as much as 7 mm of epicardial fat allows for effective irrigated-tip ablation in humans.

Predicted epicardial target sites in idiopathic VA. Real-time visualization of coronary anatomy and epicardial fat before obtaining epicardial access might be particularly important in patients with idiopathic focal arrhythmias. Based on local activation times, we could not only correctly predict the epicardial TSs but also, using the integrated MDCT, the proximity of coronary arteries and fat thickness at these TSs before epicardial access. Consequently, image integration may predict potential ablation failure and may thereby prevent unnecessary epicardial access in selected patients.

Study limitations. The comparison of successful and unsuccessful ablation sites was performed retrospectively. The validation of a cutoff value of >7 mm for epicardial fat preventing effective ablation should be performed in a prospective manner in a larger group of patients. Although MDCT-derived fat distribution cannot directly be verified using fluoroscopy, the 3-dimensional coordinates for fat meshes and coronary anatomy were derived from the same MDCT data, suggesting identical accuracy to delineate fat thickness.

The additional value of electrogram characteristics for delineation of scar was not analyzed because the current gold standard to delineate scar (contrast-enhanced magnetic resonance imaging) was not available during the procedure in all patients. However, the objective of this study was to demonstrate the clinical value of real-time image integration of MDCT-derived data and to determine the influence of epicardial fat thickness on bipolar and unipolar electrogram voltages. Therefore, only areas without evidence of scar were evaluated.

CONCLUSIONS

Real-time image integration of pre-acquired MDCT data on coronary anatomy and epicardial fat using the LM as a single landmark with EAM is safe, accurate, and feasible and available before epicardial access. One fourth of the epicardial surface is covered by >4 mm of fat, which is predominantly present at the LV superior wall and RV anterior wall. Although bipolar voltages decrease with increasing fat thickness, the exact delineation of fat based on bipolar voltage is poor and may even be worse if subepicardial scar is present. In contrast, unipolar voltages are not influenced by fat and might therefore be superior to identify scar covered by fat.

Epicardial fat >7 mm and the presence of coronary arteries are important reasons for epicardial ablation failure. The distance between ablation TSs and main coronary artery branches can be assessed by visualization of the MDCT-derived coronary anatomy. Visualization of fat thickness may facilitate interpretation of bipolar electrograms and identification of ineffective ablation sites. Finally, accurate image integration after endocardial ablation failure for focal VA may even prevent unnecessary pericardial access and thereby potential complications in selected patients.

Reprint requests and correspondence: Dr. Katja Zeppenfeld, Department of Cardiology, Leiden University Medical Center, Postal Zone C-05-P, PO Box 9600, 2300 RC Leiden, the Netherlands. *E-mail: K.Zeppenfeld@lumc.nl.*

REFERENCES

1. Saba MM, Akella J, Gammie J, et al. The influence of fat thickness on the human epicardial bipolar electrogram characteristics: measurements on patients undergoing open-heart surgery. Europace 2009;11:949–53.
2. Tung R, Nakahara S, Ramirez R, et al. Distinguishing epicardial fat from scar: analysis of electrograms using high-density electroanatomic mapping in a novel porcine infarct model. Heart Rhythm 2010;7:389–95.
3. Desjardins B, Morady F, Bogun F. Effect of epicardial fat on electroanatomical mapping and epicardial catheter ablation. J Am Coll Cardiol 2010;56:1320–7.
4. d'Avila A, Houghtaling C, Gutierrez P, et al. Catheter ablation of ventricular epicardial tissue: a comparison of standard and cooled-tip radiofrequency energy. Circulation 2004;109:2363–9.
5. van Velzen JE, Schuijf JD, de Graaf FR, et al. Diagnostic performance of noninvasive multidetector computed tomography coronary angiography to detect coronary artery disease using different endpoints: detection of significant stenosis vs. detection of atherosclerosis. Eur Heart J 2011;32:637–45.
6. Abbara S, Desai JC, Cury RC, et al. Mapping epicardial fat with multidetector computed tomography to facilitate percutaneous transepicardial arrhythmia ablation. Eur J Radiol 2006;57:417–22.
7. Berruezo A, Mont L, Nava S, et al. Electrocardiographic recognition of the epicardial origin of ventricular tachycardias. Circulation 2004;109:1842–7.
8. Daniels DV, Lu YY, Morton JB, et al. Idiopathic epicardial left ventricular tachycardia originating remote from the sinus of Valsalva: electrophysiological characteristics, catheter ablation, and identification from the 12-lead electrocardiogram. Circulation 2006;113:1659–66.
9. Valles E, Bazan V, Marchlinski FE. ECG criteria to identify epicardial ventricular tachycardia in nonischemic cardiomyopathy. Circ Arrhythm Electrophysiol 2010;3:63–71.
10. Sosa E, Scanavacca M, d'Avila A, Pilleggi F. A new technique to perform epicardial mapping in the electrophysiology laboratory. J Cardiovasc Electrophysiol 1996;7:531–6.
11. Wijnmaalen AP, van der Geest RJ, van Huls van Taxis CF, et al. Head-to-head comparison of contrast-enhanced magnetic resonance imaging and electroanatomical voltage mapping to assess post-infarct scar characteristics in patients with ventricular tachycardias: real-time image integration and reversed registration. Eur Heart J 2011;32:104–14.
12. Marchlinski FE, Callans DJ, Gottlieb CD, Zado E. Linear ablation lesions for control of unmappable ventricular tachycardia in patients with ischemic and nonischemic cardiomyopathy. Circulation 2000;101:1288–96.
13. van Huls van Taxis CF, Wijnmaalen AP, den Uijl DW, et al. Reversed polarity of bipolar electrograms for predicting a successful ablation site in focal idiopathic right ventricular outflow tract arrhythmias. Heart Rhythm 2011;8:665–71.
14. Hutchinson MD, Gerstenfeld EP, Desjardins B, et al. Endocardial unipolar voltage mapping to detect epicardial ventricular tachycardia substrate in patients with nonischemic left ventricular cardiomyopathy. Circ Arrhythm Electrophysiol 2011;4:49–55.
15. Polin GM, Haqqani H, Tzou W, et al. Endocardial unipolar voltage mapping to identify epicardial substrate in arrhythmogenic right ventricular cardiomyopathy/dysplasia. Heart Rhythm 2011;8:76–83.

Key Words: epicardial ablation ■ epicardial fat ■ MDCT integration ■ ventricular arrhythmias.

▶APPENDIX

For supplemental figures, please see the online version of this article.